Acta Metallurgica Sinica (English Letters) (2023) 36:827–838
https://doi.org/10.1007/s40195-022-01486-4

# Microstructure Characteristics and Corrugation Interface Behavior of Al/Mg/Al Composite Plate Rolled Under Large Strain

**Peng-Da Huo[1] · Feng Li[1,2,3] · Wen-Tao Niu[1] · Rong-He Gao[1] · An-Xin Zhang[1]**

Received: 25 July 2022 / Revised: 21 August 2022 / Accepted: 29 August 2022 / Published online: 28 November 2022


**Abstract**
Traditional rolled (TR) aluminum (Al)/magnesium (Mg)/aluminum (Al) composite plates have many bottlenecks such as multiple passes, low interlaminar strength, and weak mechanical properties. In this paper, the hard-plate rolling (HPR) method was used to prepare Al/Mg/Al composite plates under a single pass reduction of 60%. The results show that the ultimate tensile strength (UTS) of the composite plate obtained by hard-plate rolling is 262.3 MPa, and the percentage of total elongation at fracture ($A_t$) is 12.3%, which is 31.6% and 37.4% higher than that of the traditional rolling, respectively. It is attributed to the unique corrugated interlocking structure of the interface of the composite plate caused by hard-plate rolling. The shear texture produced by the Mg plate weakens the strong-basal texture. At the same time, the strong basal slip and the large amount of energy stored in the deformed grains provide favorable conditions for dynamic recrystallized (DRX) nucleation. The microstructure is deeply refined by DRX, and the strength and plasticity of the composite plate are improved synchronously. It provides scientific guidance for the development of high-performance lightweight composite plates and the research on hard-plate rolling technology and also has good industrial production and application potential.

**Keywords** Hard-plate rolling · Al/Mg/Al composite plate · Corrugated interface · Strength-plasticity · Strengthening mechanism

## 1 Introduction

Compared with a single metal plate, the physical and mechanical properties of the layered composite plate have been greatly improved, which makes it easier to meet the needs of diversified functions [1–3]. Among them, Al/Mg/Al composite plates are gradually being widely used in aerospace, rail transit, weapons, equipment, and other fields because of its advantages of lightweight, corrosion resistance, high strength and many complementary advantages of Al and Mg [4, 5]. At present, the pressure processing methods for preparing laminated composite plates mainly include rolling [6], extrusion [7], explosive welding [8], high-pressure torsion [9], etc.

Because it is the normal combination between the plate-layers, rolling is the more commonly used process method, and edge cracking is one of the primary defects of composite plate rolling. Wang et al. [10] proposed hard-plate rolling. The research results showed that rolling with a large reduction could be realized in a single pass, which not only reduced the rolling passes but also inhibited the generation of edge cracks defects. Zhao et al. [11] successfully prepared Al/Mg/Al composite plates by wrapping Mg plates with Al plates. Through research, it had been found that cladding rolling can reduce the probability of edge crack in the forming process and improve the formability of composite plates. Still, the bonding ability between laminates is poor.

Improving the interfacial bonding is also one of the main concerns of composite sheet rolling and forming. Increased

Available online at http://link.springer.com/journal/40195

✉ Feng Li
fli@hrbust.edu.cn

✉ Wen-Tao Niu
tao364904899@163.com

[1] School of Materials Science and Chemical Engineering, Harbin University of Science and Technology, Harbin 150040, China

[2] Key Laboratory of Micro-systems and Micro-structures Manufacturing of Ministry of Education, Harbin Institute of Technology, Harbin 150001, China

[3] Key Laboratory of Superlight Materials and Surface Technology, Ministry of Education, Harbin Engineering University, Harbin 150001, China

annealing treatment after rolling is used, thereby achieving the transition from mechanical to metallurgical bonding [12, 13]. Still, excessively thick intermetallic compounds considerably deteriorate the interfacial bonding of the annealed composite sheet. In addition, some researchers have used metal foils such as Ag and Zn sandwiched between the target laminated metal plates [14], which can inhibit the formation of original intermetallic compounds during the forming process. In contrast, the metal foil forms a new eutectic phase with the metal on both sides. The results show that the addition of metal foil can improve the interfacial bonding ability, but it has not been widely used because of the complex process and high cost. Wang et al. [15] proposed rolling Al/Mg composite plate with the corrugated roll. The composite plate with a corrugated interface was prepared by the combination of corrugated roll and flat roll. The results showed that its interface connected in corrugated form could significantly improve the interfacial bonding ability, but two passes were required to complete the rolling.

Strength and plasticity are also essential factors when rolling composite plates. Chang et al. [16] prepared Al/Mg composite plates by cumulative stack rolling, and the results showed that with the increase in the number of rolling passes, the elongation and tensile strength of the composite plates showed an increase and then a decrease. The performance of composite plate rolled in two passes is the best. The tensile strength is 235 MPa and the elongation is 13%. In addition, the research results on the properties of rolled composite plates after explosive welding showed that [17, 18] secondary rolling could significantly improve the tensile strength of composite plates, but it was still obtained at the expense of plasticity.

In summary, achieving improved mechanical properties while ensuring the formability of rolled composite plates has become a problem for many researchers. In this paper, the forming process of a hard plate rolling Al/Mg/Al composite plate was proposed. According to previous studies, it had been found that hard-rolled composite plates could be rolled in a single pass with a large reduction without edge cracks [19]. Its corrugated interface can achieve an increase in interfacial bond strength. However, the plate organization and tensile properties are still in a blank state. In this paper, the electron back-scattered diffraction (EBSD) study was carried out on the magnesium structure of the composite plate, and the effect of the structure and the corrugated interface morphology on the tensile properties was further investigated.

## 2 Experimental

The equipment used in this study was a two-roller mill (ϕ140 mm × 260 mm). As listed in Table 1, the materials used were commercially rolled AZ31B Mg alloy plate (thickness 5 mm) and AA1060 Al alloy plate (thickness 0.5 mm). The original billet was cut by mechanical cutting to (L × W) 60 mm × 30 mm. The hard plate material selected was ASTM304 stainless steel, size (L × W × H) 100 mm × 60 mm × 1 mm. Before rolling the Al, Mg billet bond surface for coarse sandpaper sanding to expose the fresh metal, and then placed in acetone solution to remove the surface oil, remove and rinse with alcohol and natural air dry. Figure 1 shows the hard-plate rolling composite plate process principle and annealing scheme. The sheet blanks were stacked sequentially in the manner shown in Fig. 1a. There was sliding friction between the roller and the plate. Before rolling, the front end of all plates shall be polished to a 15° inclination angle to ensure that the bite angle of each rolling plate was the same. One end of the plate was fixed with thin steel wire. The sample processing route was shown in Fig. 1b, and the pre-treated completed stacked plates were placed into a heat treatment furnace set to a constant temperature of 350 °C for 10 min to preheat. After the preheating, the press-down amount was adjusted to 60%, and then the laminated plate with the bound end was quickly fed into the rolling mill. Finally, the rolled composite plate was put into a furnace at 300 °C for a short period of stress relief annealing. In this experiment, the Al/Mg/Al composite plate without the hard plate was prepared by rolling in three passes (30% + 25% + 25%) under the same conditions as the mechanical properties control.

Tensile experiments were carried out using a universal tensile testing machine with a constant tensile speed of 0.1 mm/min. Tensile specimens were selected from the rolling direction–transverse direction (RD-TD) plane of the rolled plate. Three samples were selected for each group of data to be measured, and the average results were selected. Microstructure specimens were prepared in each typical part of the rolling direction – normal direction (RD-ND) plane of the plate. Scanning electron microscopy (SEM) was used to characterize the intermetallic compound, and interfacial connection morphology of the hard-plate rolled laminate. Tests were performed under an X' Pert PRO-type X-ray diffractometer with a tube voltage of 40 kV and a tube current of 40 mA, with continuous scanning of the bonded area on the Al/Mg/Al side in the range of 20°–80° and a scanning speed of 0.03°/s.

**Table 1** Composition of AZ31B Mg and AA1060 Al alloys (wt%)

| Alloys | Mg | Al | Mn | Cu | Fe | Zn | Ca |
|---|---|---|---|---|---|---|---|
| AZ31B | 95.45 | 3.9 | 0.334 | 0.05 | 0.005 | 0.81 | 0.04 |
| AA1060 | 0.03 | 99.6 | 0.03 | 0.05 | 0.35 | 0.05 | – |

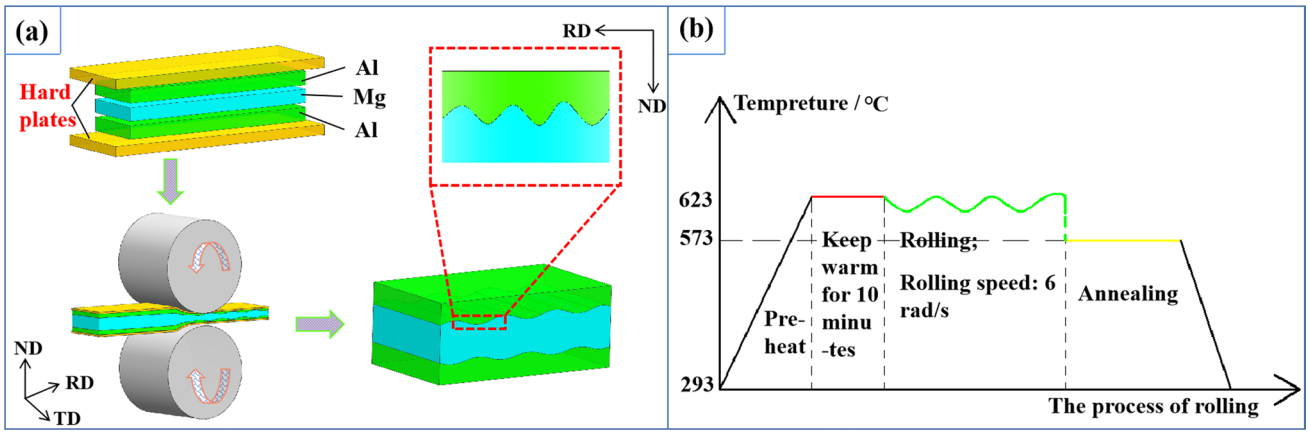


**Fig. 1** Schematic diagram of the principle of the hard-plate rolling Al/Mg/Al composite plate: **a** process principle; **b** experimental process

The EBSD specimens were wire cut with an intercept size of 8 mm × 4 mm × 2 mm. After mechanical polishing, electrolytic polishing was added to remove metal burrs from the sample surface. The sample surface was quickly cleaned using alcohol after electrolysis. Finally, the samples were tested in a Quanta 200F field emission scanning electron microscope. The scanning step size of EBSD was 1.3 μm. The scanning area was 200 μm × 200 μm. Channel 5 software was used to standardize the noise reduction in the raw data and perform EBSD data analysis.

## 3 Results

### 3.1 Interface Morphology

The interface morphology of the Al/Mg/Al composite plate obtained by hard-plate rolling is shown in Fig. 2. Due to the symmetrical distribution of the interlayer structure, Fig. 2a shows the morphology of the Al/Mg bonding interface on one side of the composite plate. Under the rolling conditions of the hard plate, the interface structure presents a wavy characteristic, and there are no defects such as pores, cracks, and apparent delamination, indicating that the interface is well bonded. The energy-dispersive spectroscopy (EDS) line scan shows the decrease of Mg element and the increase of aluminum element in Fig. 2c), indicating that element diffusion occurs at the interface during the annealing process in a short time, forming a 11 μm diffusion layer. This diffusion layer is mainly composed of intermetallic compounds. The phase analysis of the intermediate layer showed that the Mg content at point A was 42.3% and the Al content was 57.7%; the Mg content at point B was 59.1%, and the Al content was 40.9%. It can be preliminarily determined that the composition of the intermetallic compound near the Al layer is $Al_3Mg_2$, and the composition near the Mg layer is $Mg_{17}Al_{12}$ [20, 21]. To further confirm the document of the composition, an X-ray diffraction (XRD) phase analysis was performed on the bonding interface of one side of the Al/Mg/Al composite board. As shown in Fig. 2d, $Al_3Mg_2$ and $Mg_{17}Al_{12}$ diffraction peaks are formed, and the composition of the intermetallic compound is finally determined.

### 3.2 Mechanical Properties

Under the condition of combination matching of Al plate 0.5 mm and Mg plate 5 mm thickness, the differences in mechanical properties of the rolled composite plate with and without hard plate were compared. Figure 3a compares unidirectional tensile mechanical properties between traditional rolling and hard-plate rolling Al/Mg/Al composite plate and Mg plate after automatic stripping of the Al layer.

As shown in Fig. 3a, the ultimate tensile strength (UTS) and $A_t$ of traditional rolled composite plates are only 179.3 MPa and 7.7%, respectively. The UTS and $A_t$ of the hard-plate rolled composite plate are up to 262.3 MPa and 12.3%, respectively, which are 31.6% and 37.4% higher than those of the former. The comprehensive mechanical properties are significantly improved.

The stress–strain curve obtained from the tensile test of the traditional rolled composite plate almost coincides with the stripped magnesium plate under the same conditions, indicating that the UTS and $A_t$ of the two are similar. It is consistent with the tensile test results of mechanical properties of traditional rolled composite plates [22]. The results show that the Al plate on both sides of the composite plate is skinny (approximately 300 μm), and the tensile properties of composite plates are mainly determined by the properties of Mg plates [23]. Compared with traditional rolling, the UTS and $A_t$ of the Mg plate after stripping off the hard-plate rolling clad plate are improved, and the $A_t$ is improved more significantly. Therefore, it can be preliminarily learned that

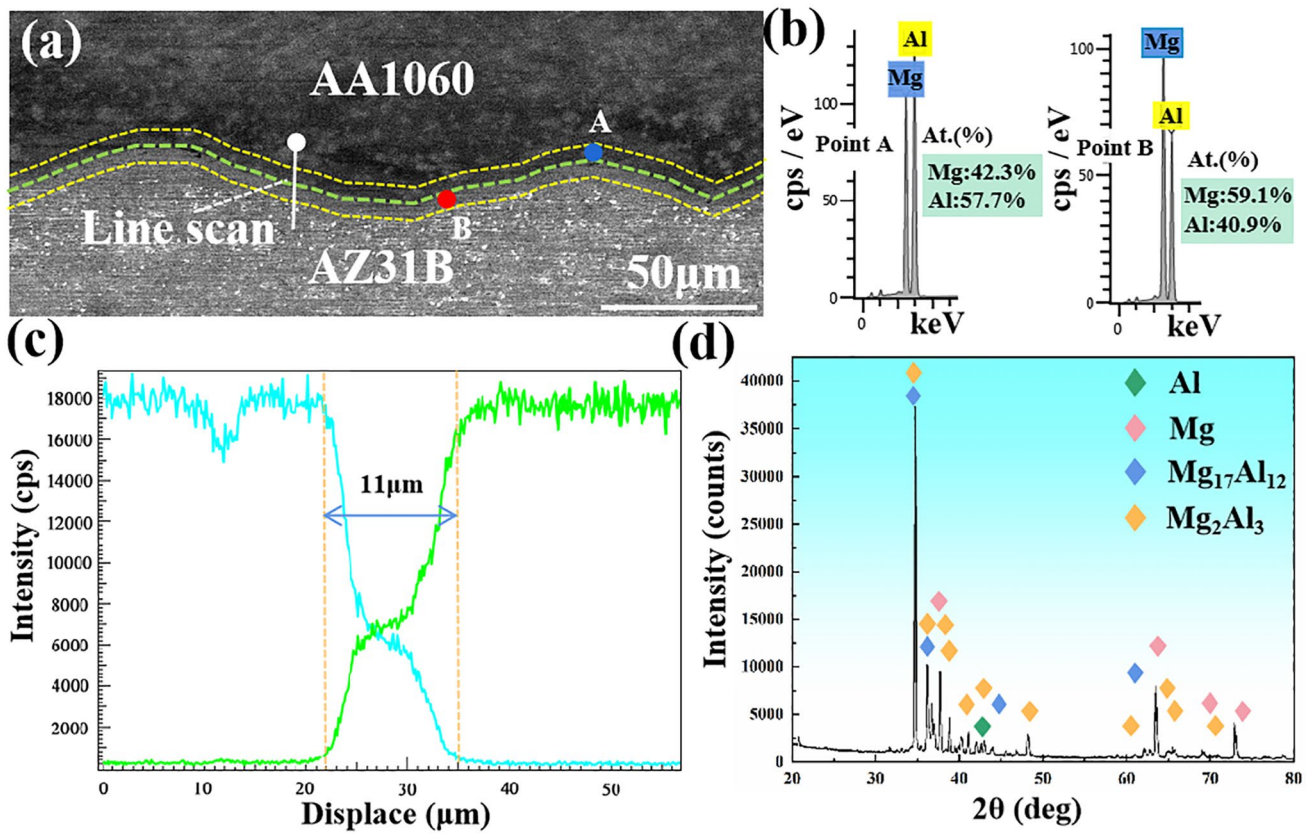


**Fig. 2** Morphology of the interface of the composite plate: **a** morphology of the Al/Mg interface; **b** A and B point scanning at the interface; **c** line scan of the diffusion layer; **d** XRD at the interface

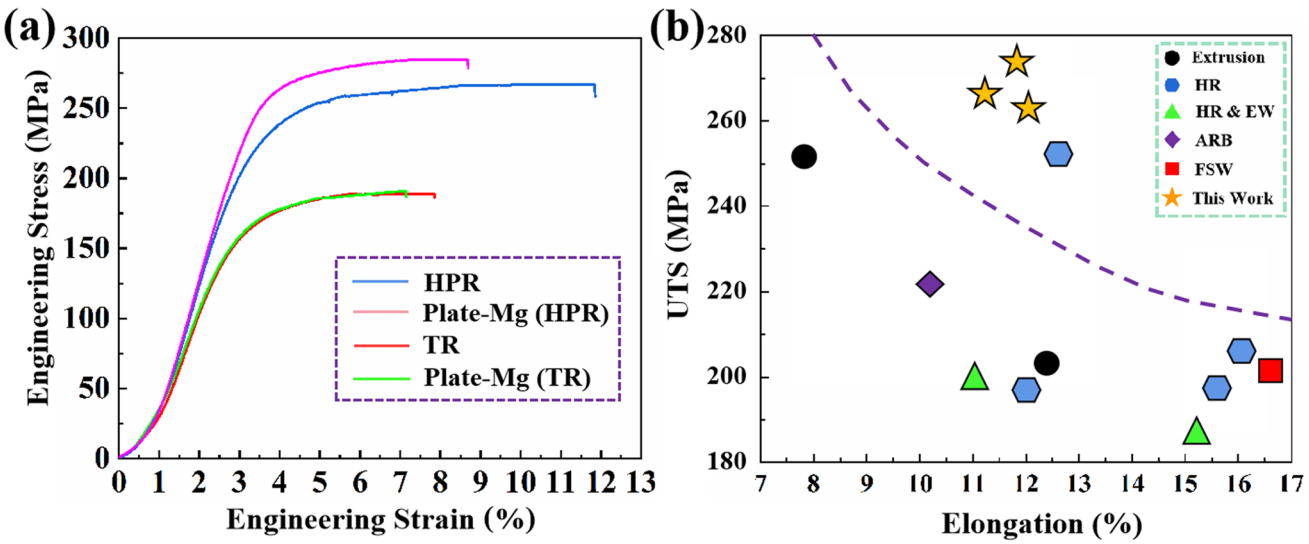


**Fig. 3** Tensile properties: **a** engineering stress–strain; **b** comparison of UTS and elongation of Al/Mg/Al composite plate under different processes

the double increase in plasticity and strength of hard-plate rolled composite plate is not only caused by the improvement of Mg plate properties but also the change in interface structure plays an important role.

Figure 3b compares UTS and $A_t$ of Al/Mg/Al composite plates obtained under different process conditions. These forming methods include extrusion [24, 25], friction stir welding (FSW) [26], hot rolling & explosive welding (HR & EW) [27, 28], hot rolling (HR) [29–32], and accumulative rolling bonding (ARB) [33]. Due to the difference in process conditions (plate thickness, materials, etc.), the performance standards of composite plates prepared by traditional hot rolling are not unified. However, the average level is maintained at the UTS of 232.5 MPa and the $A_t$ of 10.2%. For the composite plate, hot rolled after explosive welding, its tensile strength is greatly improved, but it is obtained by sacrificing plasticity, so the elongation is poor. It is similar to the performance of an accumulative rolling bonding composite plate. Al/Mg/Al composite plate prepared by friction stir welding and extrusion process improves the elongation of the plate, but the strength is relatively weak. The Al/Mg/Al composite plates prepared by these methods have mutual constraints on tensile strength and $A_t$. On the contrary, the double gain effect of tensile strength and elongation is realized in the mechanical properties of the hard-plate rolled clad plate.

Figure 4 shows the tensile fracture morphology of the Al/Mg/Al composite plate. It can be seen from the RD-ND plane that the fracture of the Mg plate presents a V-shaped structure, as shown in Fig. 4a. From the partial enlargement, we can see that due to the effect of the corrugated interface, the Al/Mg layer is well bound away from the fracture, and there is no delamination parallel to the extension axis. The small degree of interface cracking also indirectly indicates the strong interface bonding effect of the hard-plate rolled composite plate. As shown in Fig. 4b, apparent dimples appear in the Mg plate after rolling, showing the characteristics of ductile fracture. At the same time, a large number of dissociation steps can be seen at the necking of the Al plate, and the number of dimples is small. The results of the fracture scanning experiment perfectly accord with the results of the best mechanical properties of Al/Mg/Al composite plate obtained by hard plate rolling.

To further clarify the effect and mechanism of the corrugated interface on the tensile properties of the Al/Mg/Al composite plate, the segmented characterization method was used to observe the change in the interface morphology of corrugated interface in the tensile process. Tensile samples were prepared at the same position in the hard-plate rolled composite plate under the same conditions, and test the tensile properties under 3%, 6%, 9%, and 12% strain conditions. The tests were repeated many times under each strain condition, and the average value was taken, as shown in Fig. 5. To exclude the influence of intermetallic compounds, the tensile samples used in the test were all non-annealed plates, and the metallurgical bonding effect at the submicron level caused by rolling could be ignored [34]. As shown in Fig. 5, when the strain is 3%, the Al/Mg bonding interface is closely connected, corrugated, and free of defects. When the strain is 6%, the ripple interface can be seen with increasing strain, the wave crest and trough are small, but the ripple shape can still be observed. When the strain reaches 9%, the corrugated interface disappears, and the composite plate joint

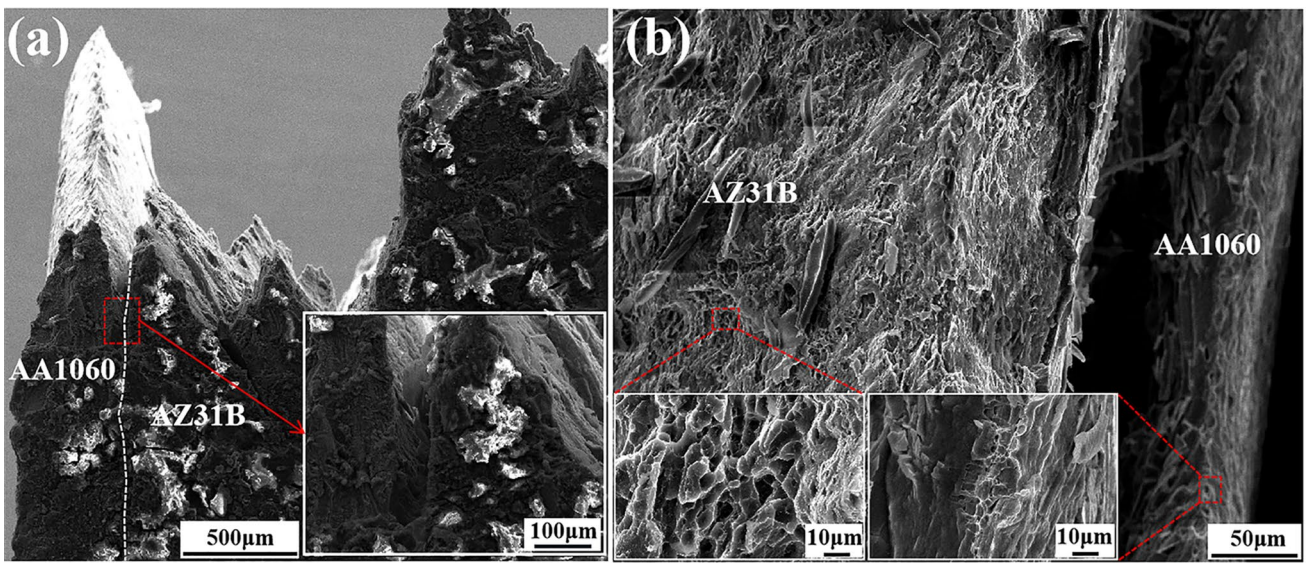


**Fig. 4** Fracture morphology: **a** interface fracture morphology (RD-ND); **b** interface fracture morphology (TD-ND)

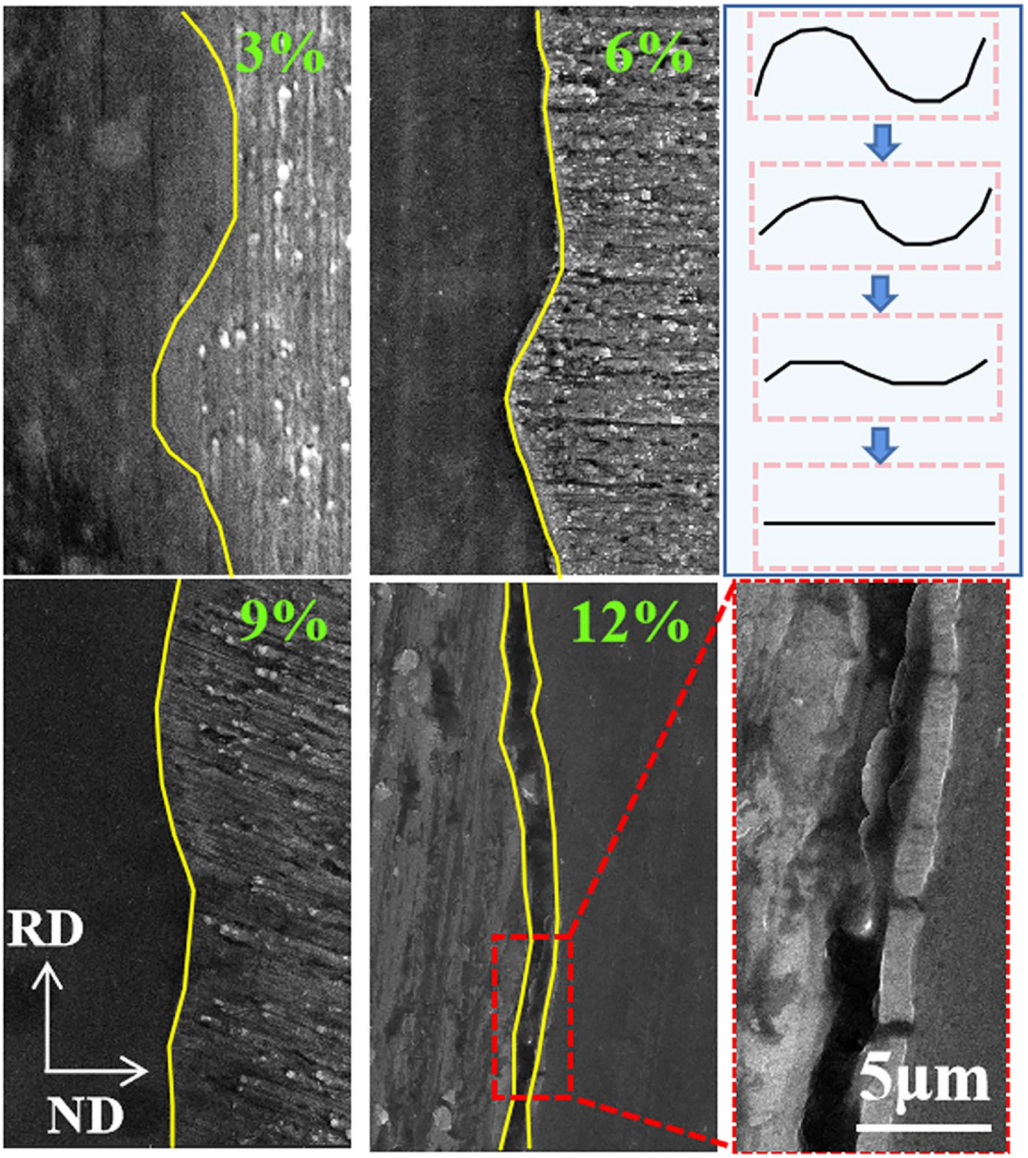


**Fig. 5** Interface morphologies under different strains

is closely connected in concave-convex fluctuation. When the strain reaches 12%, cracks can be seen at the Al/Mg bonding interface, as shown in Fig. 5. The locally enlarged view shows that the thinner diffusion layer produced during rolling will also make transverse fracture. As shown in the tensile interface morphology of Fig. 5, the corrugated interface is under strain $\varepsilon < 6\%$ of cases, and the change speed of ripple shape is slow. In the 6%–9% stage, the change degree of the corrugated interface increases with strain. From the original corrugated shape, under tensile stress, the crest and trough are gradually elongated and degenerated into a flat shape, and finally cracks occur at the interface under large strain conditions.

### 3.3 Microstructure

The test results of RD-ND surface texture in the Mg plate after stripping off the hard-plate rolled composite plate are shown in Fig. 6. As shown in Fig. 6a, the microstructure is mainly composed of deformed grains. Different from the equiaxed grains formed by conventional rolling, hard-plate rolling can convert the shear stress into compressive stress. In the deformation process, the grains have no time to break and refine, and become slender under the combined action of large compressive stress and tensile stress. This loading mode makes the microstructure formed by hard-plate rolling vary greatly. Figure 6c shows

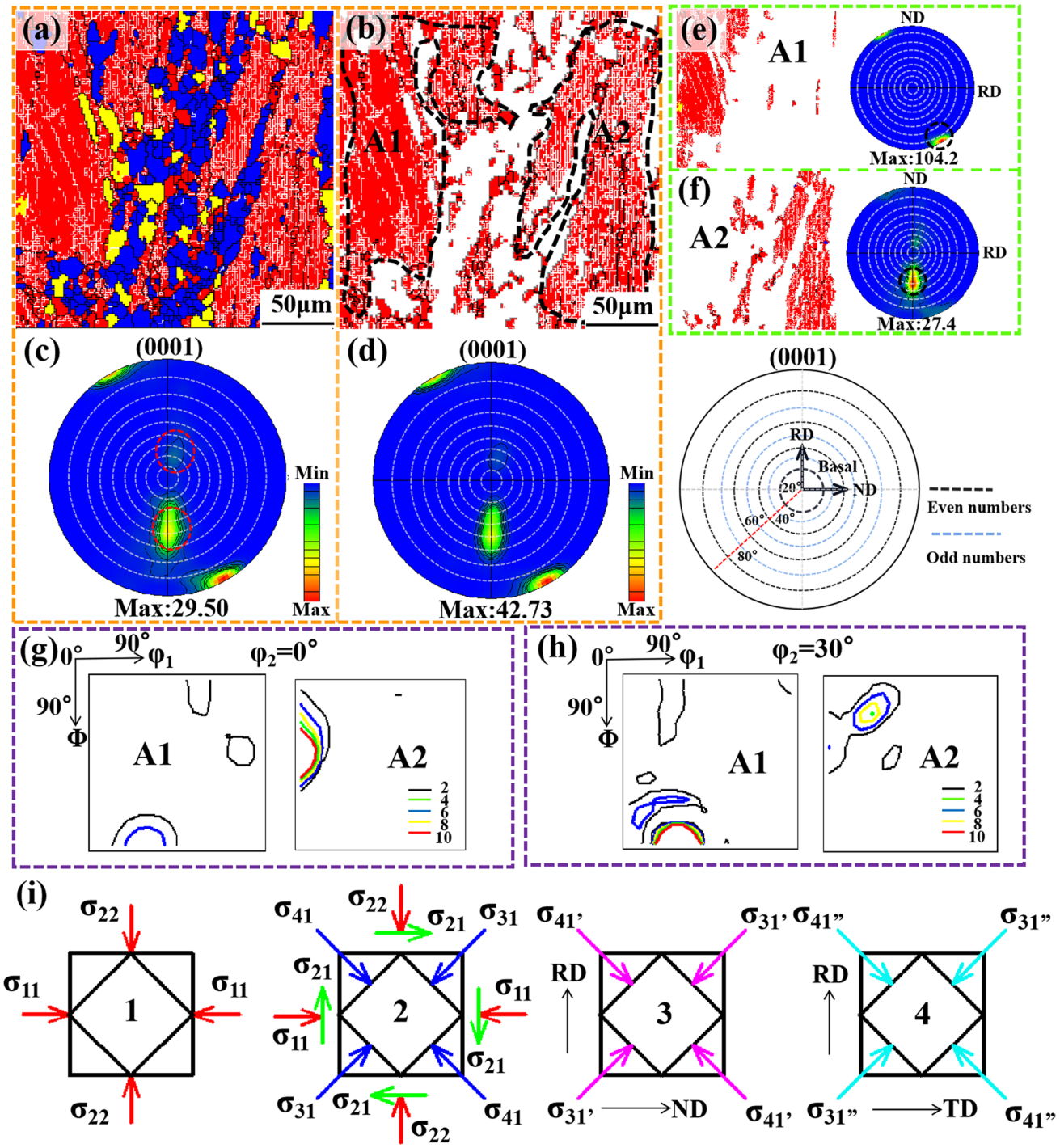


**Fig. 6** Texture of deformed grains: **a** recrystallization; **b** deformed grains; **c** PF of **a**; **d** PF of **b**; **e** PF of A1; **f** PF of A2; **g**, **h** ODF graphs; **i** plane strain–stress of hard-plate rolling

the {0001} polar figure (PF) of the tissue, and its texture type is mixed texture, including basal texture and deflection texture toward TD. It should be noted that by analyzing the texture of deformed grains, it is found that the texture type is similar to the overall structure shown in Fig. 6a (Fig. 6d). This indicates that deformed grains play a major role in influencing texture types. To further analyze the evolution of deformed grains, as shown in Fig. 6b, they are divided into two parts, A1 and A2. These two deformed grains constitute the texture type of Fig. 6d. As shown in Fig. 6e, the texture at A1 presents a basal texture inclined from ND to RD, and the high-strength areas

(red and yellow) are distributed at the two poles with high texture strength. The texture at A2 deflects 37.5° to TD, the *c*-axis of the deformed grain deflects preferentially to TD, and the texture strength is 27.4, which significantly weakens the texture strength. The orientation distribution function (ODF) of Fig. 6g and h is intercepted from the Euler angle of common Mg alloys $\varphi_2 = 0$, and $\varphi_2 = 30$ to analyze the texture composition of AZ31B in hard plate rolled composite plate. As visible in Fig. 6, when $\varphi_2$ is 0°, the extreme density intensity of A1 texture is small, and there is no obvious texture type, while A2 aggregates at Euler angle ($\varphi_1$, $\phi$, $\varphi_2$) (12, 38, 0). The main texture components of A1 and A2 are located at Euler angles ($\varphi_1$, $\phi$, $\varphi_2$) (23, 85, 30) and (25, 25, 30). The strength of the former is higher, which is consistent with the PF analysis.

Figure 7 shows a schematic diagram of the recrystallization of Mg plate in the hard-plate rolled composite plate. As shown in Fig. 7e, the EBSD sample was prepared at the center of the Mg plate of the composite plate. Figure 6a shows that the hard-plate rolled Mg plate comprises coarse grain and fine grain nonuniform structures. Red represents deformed grains, and blue represents recrystallized grains. As shown in Fig. 7a, several fine dynamic recrystallized (DRX) grains coexist around the coarse deformed grains to form a "necklace" structure. To further explain the recrystallization mechanism, two typical deformed grains with different grain orientations and their surrounding fine grains are named B1 and C1, respectively in Fig. 7a, and the orientation difference distribution in the two coarse grains B1 and C1 is measured. As seen in Fig. 7e, as shown in

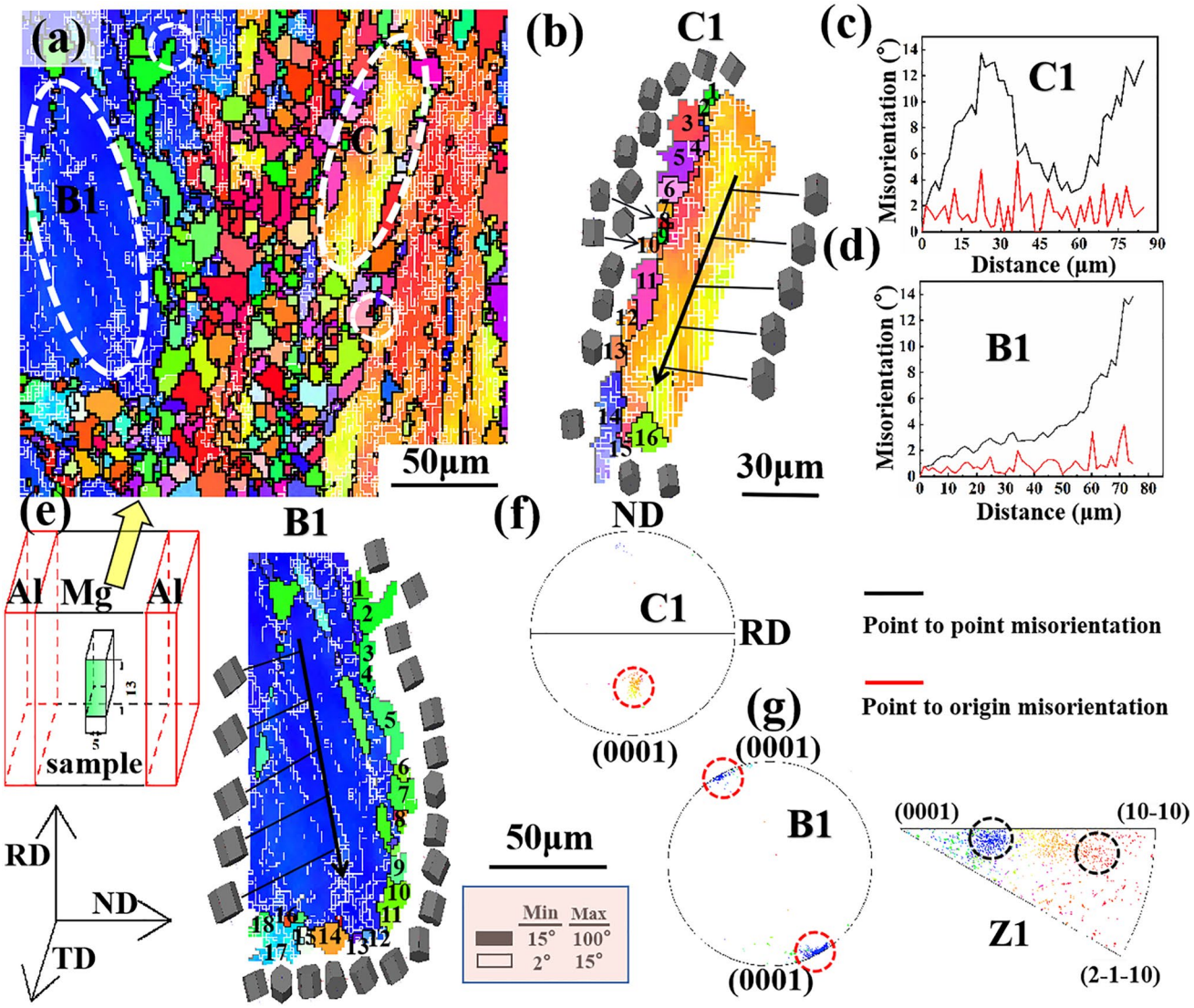


**Fig. 7** Recrystallization behavior: **a** IPF map; **b** local amplification of C1; **c**, **f** angle orientation difference and PF, respectively of C1; **e** sampling method and grains of B1; **d**, **g** angle orientation difference and PF, respectively of B1

the three-dimensional crystallographic diagram along the arrow direction in the B1 grain, the degree of grain rotation around the *c*-axis is small, which is consistent with the curve in Fig. 6d. From the change in grain angle from point to point, the grain rotation angle is approximately 3°, and the cumulative orientation difference between point and origin gradually increases to 14°, indicating the continuous change in orientation in deformed grains. As shown in the partial enlargement of ellipse C1 in Fig. 7a and Fig. 7b, the inverse pole figure (IPF) color of the C1 grain is composed of orange, red and yellow. Compared with B1 grain, the number of low-angle grain boundaries (LAGBs) in the grain increases significantly, and the dislocation density increases.

It is shown in Fig. 7c that the orientation gradient inside the grain is more pronounced. According to the measured orientation difference distribution, an apparent orientation gradient is formed in coarse crystal C1. At the same time, there are many LAGBs. Therefore, either B1 or C1 can become the initial grain formed by recrystallization. The sub-crystals in coarse grains can capture moving dislocations, increase the orientation difference, and evolve into high-angle grain boundaries (HAGBs). Then the high-angle grain boundary migrates to eliminate some LAGBs, and finally obtain fine recrystallized grains, a typical continuous DRX feature [35, 36]. In addition, there are unique grains around the coarse grains of B1 and C1. The grains marked by circles in Fig. 7a bend and bulge at some grain boundaries to form serrated fine DRX, characteristic of discontinuous DRX [37, 38].

## 4 Discussion

To further explore the internal reasons for the improvement of the properties of hard-plate rolled clad plate, it is expounded from two aspects: microstructure and corrugated interface.

### 4.1 Microstructure

#### 4.1.1 Shear Texture

It is shown from the IPF in Fig. 7 and the recrystallization in Fig. 6 that the deformed grains mainly have two-grain orientations, one is (10–11) conical orientation, and the other is (0002) basal orientation. The fine-recrystallization orientation is relatively free. The front and back sliding zones of traditional rolling have the same length. The positive and negative shear effects on the rolled plate surface can be largely offset. However, for hard-plate rolling, the excessive reduction will increase the length of the rear sliding zone, resulting in an eccentric load of shear force, resulting in a nonuniformity of deformation. The traditional rolling method of small reduction and multiple passes makes the plate stress uniform, but this paper adopts one pass large reduction to form. This nonuniform rolling makes the plastic flow velocity and displacement of each part of the deformed metal different. The nonuniform plastic flow will cause shear stress between the deformed parts, resulting in the emergence of shear texture. The effect of external hard plate intensifies the formation of uneven deformation texture, as shown in Fig. 6e and f. Figure 6i shows the stress analysis of the hard-plate rolled composite Mg plate. At the center of the rolled plate, the plate bears the tensile stress in the rolling direction (RD) ($\sigma_{11} > 0$) and the compressive stress in the ND of the plate surface ($\sigma_{22} < 0$). At the place far away from the center, the shear stress $\sigma_{21}$ brought by the roll is increased (No. 1 to No. 2 in Fig. 6i). Since the hard plate can transform the shear stress part into compressive stress, the principal stress state of the (RD-TD) plane is deflected (changes No. 2 to No. 3 in Fig. 6i). At the same time, the plate in TD also has a large extension under the action of the hard plate, and the stress changes from No. 2 to No. 4 in Fig. 6i appear. Due to this change in stress state, when the base slip system of deformed grain A1 starts, it will deflect in RD. Although the shift in orientation is limited, it will produce a certain shear strain in deformation and rotation. The shear strain will be hindered by the adjacent grains with other orientations, and the deformed grain B1 of the conical slip system will also produce the corresponding shear strain. However, the slip system where A1 is located bears a higher slip amount than the B1 slip system with a smaller orientation factor due to its high orientation factor. The two slip systems start alternately, resulting in a gradual decrease in the total shear strain, and finally, a mixed texture, as shown in Fig. 6 is formed. This mixed texture composed of shear texture greatly weakens the strength and improves the properties of the Mg plate.

#### 4.1.2 Recrystallization

Hard-plate rolling can realize the forming of the Al/Mg/Al composite plate with large reduction in a single pass. Larger plastic deformation will cause entanglement and stacking of dislocations in grains. The internal mechanism of dislocation recrystallization will promote the formation of dislocation dynamically. In addition, the hard plate plays the role of heat preservation in the rolling process, making recrystallization easier to form.

Figure 8 shows Schmid factor and kernel average misorientation (KAM) of Mg plate tissue. KAM reflects the degree of homogenization of plastic deformation of the material [39], as shown in Fig. 8a. Through calculation, it is found that the necessary geometric dislocation density of coarse deformed grains (B1, C1) can reach 0.26, which is much larger than that of the surrounding fine grains. This high

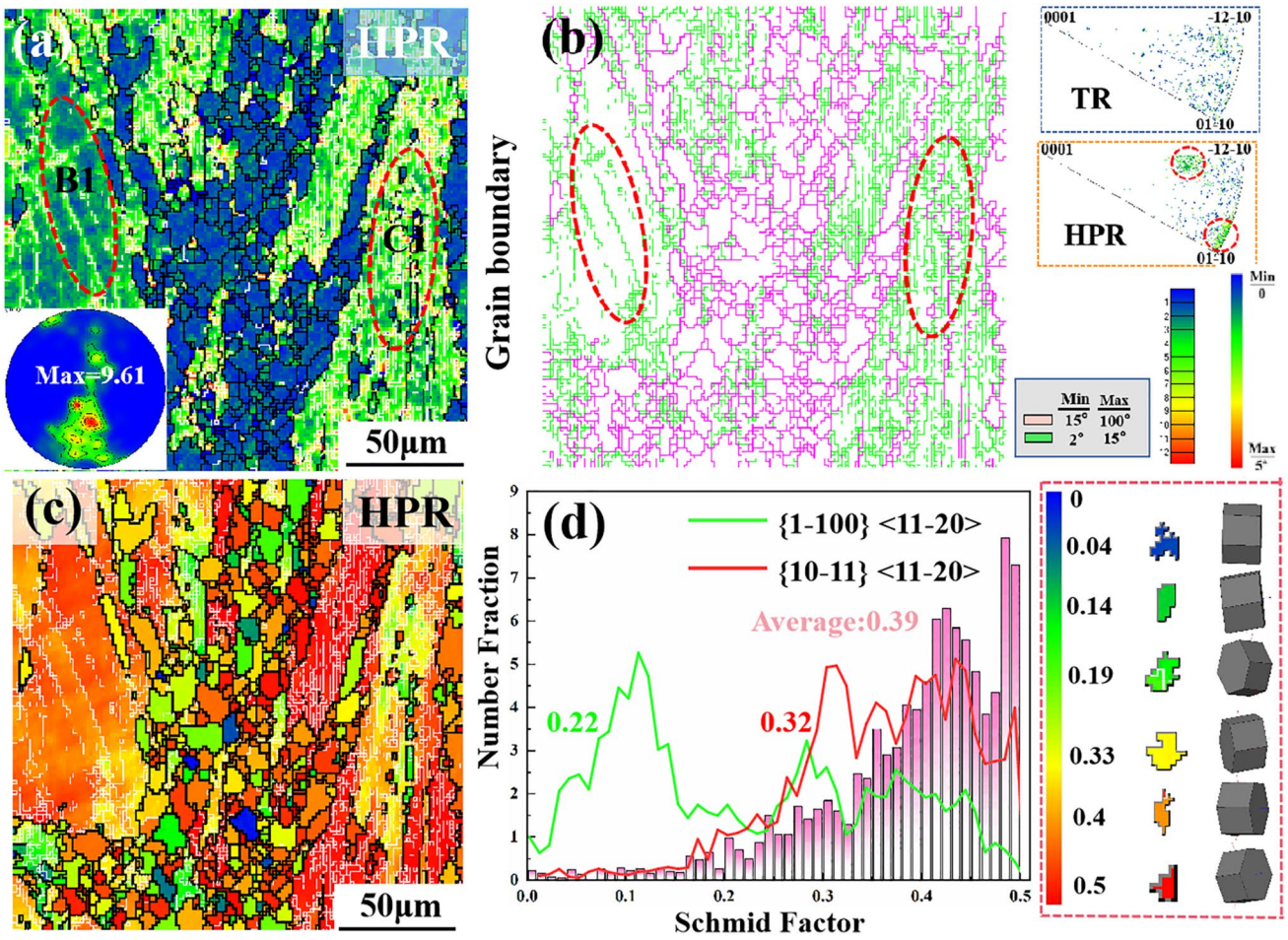


**Fig. 8** KAM and Schmid factor maps: **a** KAM map; **b** grain boundaries map; **c** Schmid factor (SF) map; **d** SF distribution curve

residual strain will become the starting point of recrystallization in the subsequent processing process. The observation shows that a large number of low-angle grain boundaries are also distributed in these deformed grains. Due to the high diffusion rate at the grain boundary of Mg alloy, the dislocations accumulated on the sub grain boundary can be absorbed by these grain boundaries, to accelerate the DRX process. As shown in Fig. 7a, the residual strain of B1 grain is smaller than that of C1 grain, and the number of sub grain boundaries is less. However, the DRX behavior can also be realized [40]. However, the higher local strain of C1 will first become the nucleation point of recrystallization, and the dispersed sub grain boundary will be transformed into recrystallization during further deformation, to decompose the deformed grains and realize the refinement of coarse grains. In addition, the cumulative orientation difference angle in the deformed grains also reflects the progress of DRX (Fig. 7). Both continuous DRX and discontinuous DRX can realize grain refinement and significantly improve the service performance of composite plates. At the same time, the *c*-axis of recrystallized grains is no longer a single row to ND, but forms a preferred orientation. As shown in Fig. 8a, the bottom left of KAM shows the recrystallization PF, showing a non-basal texture deflected towards TD, forming a bimodal texture deflected from ND to TD together with the deformed grains (Fig. 6c). The maximum texture density is only 9.61, so recrystallization can weaken the texture.

Schmid factor is closely related to the critical shear stress, which can fully reflect the difficulty of starting the slip system in metal deformation. Interestingly, the grains with higher SF are mainly deformed grains, which have greater deformation degree and more LAGBs than the recrystallized grains with lower SF, which is similar to the results of KAM. Figure 7b shows a comparison diagram of SF of base slip system, prismatic slip system, and pyramidal slip system. The histogram shows the SF of base slip, with an average value of 0.39. The {10–11} < 11–20 > pyramidal slip is 0.32, and the {1–100} < 11–20 > prismatic slip is only 0.22. Therefore, basement slip mainly occurs in the process of deformation. The energy required for recrystallization can be provided by substrate slip [41]. The substrate slip Schmid coefficient of microstructure is high, mainly distributed

between 0.3 and 0.5 (Fig. 8b).The grains with high SF have high energy storage in the base slip process, and DRX occurs in these grains to promote grain refinement.

### 4.2 Corrugated Interface

The hard plate can change the stress state of the rolled plate in the rolling process, so the metal at the interface is not only plastically deformed along RD under the action of shear stress but also subjected to the compressive stress exerted by the hard plate. The nonuniform extrusion flow at the Al/Mg metal interface [42–44] forms a special corrugated interface structure. The corrugated interface is different from the flat interface of traditional rolling. It is composed of continuously changing peaks and troughs, as shown in Fig. 2. Because the composite plate is quenched after rolling, the influence of diffusion layer and weak metallurgical bonding is excluded. Therefore, the corrugated interface becomes the main way to affect the bonding performance of the interface. During the tensile property test, the peaks and troughs at the interface gradually become flat until the whole tends to be flat, as shown in Fig. 4b. Therefore, in the drawing process of the corrugated interface, compared with the composite plate with flat interface in the traditional sense, the process of corrugated flattening is increased. This change increases the tensile stroke in the plastic deformation of the composite plate, so the elongation increases significantly. It is worth pointing out that during the tensile process, the corrugated interface in the medium strain zone to the high strain zone tends to be flattened without cracks and other defects. After the interface reaches flat, continue to stretch and load. The composite plate soon reaches and exceeds the tensile strength, resulting in cracks until fracture, which shows that the corrugated interface formed by hard plate rolling promotes the improvement of the plasticity of the composite plate.

### 4.3 Strengthening Mechanism

Figure 3b compares the properties of composite plates obtained under different conditions. The Al/Mg/Al composite plate prepared in this paper can achieve the double improvement of plasticity and strength. By analyzing the microstructure of the Mg plate, it is found that the shear texture can weaken the overall texture strength of the Mg plate. It plays a part in improving the plasticity of composite plates. In addition, the Schmid factor of base slip is large, and the base is easy to slide in the drawing process, which also plays a role in strengthening the elongation of the plate. Further analysis shows that in Fig. 3a, compared with traditional rolling. However, the plasticity of the Mg plate has been greatly improved. The elongation of the composite plate is still slightly lower than that of the hard-plate rolling. The performance difference mainly depends on the corrugated interface formed by hard-plate rolling composite plate. This special connection structure further improves the plasticity of composite plate. The corresponding traditional rolling does not enhance the plasticity of composite plate compared with Mg plate, which can better explain the role of corrugated interface.

In terms of tensile strength, it is necessary to plug a sufficient number of dislocations in the grain during the tensile process, to provide the necessary stress. The activation of dislocation sources in adjacent grains can produce macroscopically visible plastic deformation. Decreasing the grain size can increase the number of dislocation movement obstacles and further realize fine grain strengthening [45]. The energy storage in the grain of Mg plate under the action of hard plate is large, which promotes the formation of recrystallization and refines the grain [46]. For many sub-grains in deformed grains, the role of the sub-grain boundary is similar to that of the grain boundary. Many LAGBs can hinder the dislocation movement, reduce the stress concentration at the end of the slip band and reduce the probability of transverse fracture of the plate due to the stress concentration. Therefore, compared with traditional rolling, hard-plate rolling can improve the tensile strength of the Mg plate. The thickness of the Al plate after rolling is only 300 μm. It has little effect on the improvement of strength and plasticity.

## 5 Conclusions

1. The results show that the hard-plate rolling method can realize a single pass and large reduction to manufacture Al/Mg/Al composite plate, without defects such as porosity, cracks, and delamination, and the interface bonding quality is good. The interface structure of the laminate is interlocked and corrugated, which provides a new idea for the forming and manufacturing of high-performance lightweight composite plate.
2. Compared with traditional rolling, the UTS and $A_t$ of Al/Mg/Al composite plate rolled by the hard plate under the same conditions are increased by about 30%, and the double increase effect of mechanical properties is realized. The tensile property test shows that with the increase in the strain of the composite plate, the deformation process of the interface structure from corrugated to flat first appears, which is also one of the incentives to improve the elongation.
3. The changing trend of UTS and $A_t$ of the traditional rolled composite plate is consistent with that of stripped Mg plate under this condition, indicating that Mg plate plays an important role in the overall performance of composite plate. The UTS and $A_t$ of rolled composite plate and stripped Mg plate are significantly improved,

and the elongation of composite plate is significantly greater than that of the latter, indicating that the corrugated interlocking interface structure plays a role.

4. Hard-plate rolling improves the energy storage in the deformed grains in the Mg plate after composite plate stripping, and many LAGBs provide nucleation points for recrystallization. The Schmid factor of base slip is high, which provides energy, promotes the formation of recrystallization, and realizes the refinement of microstructure. Secondly, because the hard plate changes the stress state of the plate during rolling, the shear texture greatly weakens the overall texture of the plate in strength and improves the plasticity of the plate.

**Acknowledgements** This work was supported by the Key Laboratory of Micro-systems and Micro-structures Manufacturing of Ministry of Education, Harbin Institute of Technology (2020KM005).

## Declarations

**Conflict of interest** The authors state that there are no conflicts of interest to disclose.

## References

[1] M. Song, X.D. Hu, Y.C. Yang, Materials **12**, 3489 (2020)
[2] Q. Lei, H.F. Huang, F.F. Han, G.H. Lei, J. Mater. Eng. Perform. **29**, 3974 (2020)
[3] P. Ji, X.D. Ma, R.Z. Wu, L.G. Hou, J.H. Zhang, X.L. Li, M.L. Zhang, Phys. Met. Metallogr. **120**, 447 (2019)
[4] X.P. Zhang, T.H. Yang, S. Castagne, J.T. Wang, Mater. Sci. Eng. A **528**, 1954 (2011)
[5] H.P. Zheng, R.Z. Wu, L.G. Hou, J.H. Zhang, M.L. Zhang, J. Magnes. Alloy. **9**, 1741 (2020)
[6] J.H. Tang, J.W. Geng, C.J. Xia, M.L. Wang, D. Chen, H.Y. Wang, Materials **12**, 3626 (2019)
[7] Y.S. Lei, H. Yan, Z.F. Wei, J.J. Xiong, P.X. Zhang, J.P. Wan, Z.L. Wang, J. Cent. South. Univ. **28**, 2269 (2021)
[8] B.B. Zhou, C.Y. Zhou, L. Chang, X.C. Yu, C. Ye, B.J. Zhang, Compos. Struct. **236**, 111845 (2020)
[9] J.Y. Song, J.S. Ha, I.K. Kim, S.I. Hong, Adv. Mater. Res. **625**, 323 (2013)
[10] Z.Z. Jin, M. Zha, H.L. Jia, P.K. Ma, S.Q. Wang, J.W. Liang, H.Y. Wang, J. Mater. Sci. Technol. **81**, 219 (2021)
[11] Z.L. Zhao, Q. Gao, J.F. Hou, Z.W. Sun, F. Chen, J. Magnes. Alloys **4**, 242 (2016)
[12] Z.Q. Chen, L. Wei, Y. Bin, B. Zhou, Rare Metal. Mater. Eng. **44**, 587 (2015)
[13] J.S. Kim, K.S. Lee, Y.N. Kwon, B.J. Lee, Y.W. Chang, S. Lee, Mater. Sci. Eng. A **628**, 1 (2015)
[14] H.T. Zhang, J.Q. Song, Mater. Lett. **65**, 3292 (2011)
[15] T. Wang, Y. Wang, L.P. Bian, Q.X. Huang, Mater. Sci. Eng. A **765**, 138318 (2019)
[16] H. Chang, M.Y. Zheng, C. Xu, G.D. Fan, H.G. Brokmeier, K. Wu, Mater. Sci. Eng. A **543**, 249 (2012)
[17] W.W. Yang, X.Q. Cao, L.F. Wang, Z.Q. Chen, W.X. Wang, D.Y. Wang, Mater. Res. **21**, 6 (2018)
[18] M.X. Xie, L.J. Zhang, G.F. Zhang, J.X. Zhang, Z.Y. Bi, P.C. Li, Mater. Des. **87**, 181 (2015)
[19] P.D. Huo, F. Li, Y. Wang, X.M. Xiao, Int. J Adv. Manuf. Technol. **118**, 55 (2022)
[20] E. Hajjari, M. Divandari, S.H. Razavi, T. Homma, S. Kamado, Intermetallics **23**, 182 (2012)
[21] S.M. Emami, M. Divandari, E. Hajjari, H. Arabi, Int. J. Cast. Metals. Res. **26**, 43 (2013)
[22] H.H. Nie, W. Liang, H.S. Chen, F. Wang, T.T. Li, C.Z. Chi, X.R. Li, J. Alloy. Compd. **781**, 696 (2018)
[23] J.S. Kim, H.L. Dong, S.P. Jung, K.S. Lee, K.J. Kim, H.S. Kim, B.J. Lee, Y.W. Chang, J. Yuh, S. Lee, Sci. Rep. **6**, 26333 (2016)
[24] L. Chen, J.W. Tang, G.Q. Zhao, C.S. Zhang, X.R. Chu, J. Mater. Process. Technol. **258**, 165 (2018)
[25] J.W. Tang, L. Chen, G.Q. Zhao, C.S. Zhang, J.Q. Yu, J. Alloy. Compd. **784**, 727 (2019)
[26] P. Pourahmad, M. Abbasi, Trans. Nonferrous Met. Soc. China **23**, 1253 (2013)
[27] V.V. Sagaradze, N.V. Kataeva, S.Y. Mushnikova, O.A. Khar'Kov, G.Y. Kalinin, V.D. Yampol'Skii, Phys. Met. Metallogr. **115**, 202 (2014)
[28] Z.Q. Chen, D.Y. Wang, X.Q. Cao, W.W. Yang, W.X. Wang, Mater. Sci. Eng. A **723**, 97 (2018)
[29] T. Wang, S. Li, H. Niu, C. Luo, X.B. Ma, Y.M. Liu, J.C. Han, M.U. Bashir, J. Mater. Res. Technol. **9**, 5840 (2020)
[30] K.S. Lee, Y.S. Lee, Y.N. Kwon, Mater. Sci. Eng. A **606**, 205 (2014)
[31] H.P. Zheng, J.L. Yang, R.Z. Wu, T.Z. Wang, L.G. Hou, M.L. Zhang, S. Betsofen, B. Krit, Adv. Eng. Mater. **18**, 1792 (2016)
[32] Y. Yu, X.Z. Xue, Z.H. Lu, T.Y. Li, C. Ma, P.F. Yan, B. Yan, Int. J. Mod. Phys. B **34**, 2040052 (2019)
[33] J.F. Nie, M.X. Liu, F. Wang, Y.H. Zhao, Y.S. Li, Y. Cao, Y.T. Zhu, Materials **9**, 951 (2016)
[34] A.O. Bakke, L. Arnberg, Y.J. Li, Mater. Sci. Eng. A **810**, 140979 (2021)
[35] P. Xu, J.M. Yu, Z.M. Zhang, Materials **12**, 2773 (2019)
[36] S. Dai, F. Wang, Z. Wang, Z. Liu, P.L. Mao, J. Mater. Sci. **55**, 375 (2020)
[37] B.C. Xie, B.Y. Zhang, H. Yu, Y.Q. Ning, Met. Mater. Int. (2022). https://doi.org/10.1007/s12540-020-00847-x
[38] Z.M. Yan, J. Zheng, J.X. Zhu, Z.M. Zhang, Q. Wang, Metals **10**, 1102 (2020)
[39] Y.Q. Chi, C. Xu, X.G. Qiao, M.Y. Zheng, J. Alloy. Compd. **789**, 416 (2019)
[40] H. Zhang, M. Zha, T. Tian, H.L. Jia, D. Gao, Z.Z. Yang, C. Wang, H.Y. Wang, Mater. Sci. Eng. A **808**, 140920 (2021)
[41] Y.K. Li, M. Zha, J. Rong, H.L. Jia, Z.Z. Jin, H.M. Zhang, P.K. Ma, H. Xu, T.T. Feng, H.Y. Wang, J. Mater. Sci. Technol. **88**, 215 (2021)
[42] G.Y. Li, W.M. Jiang, F. Guan, J.W. Zhu, Y. Yu, Z.T. Fan, J. Magnes. Alloy. **10**, 1075 (2022)
[43] G.Y. Li, W.C. Yang, W.M. Jiang, F. Guan, H.X. Jiang, Y. Wu, Z.T. Fan, J. Mater. Process. Technol. **265**, 112 (2019)
[44] Z. Zhang, W.M. Jiang, G.Y. Li, J.L. Wang, F. Guan, G.L. Jie, Z.T. Fan, J. Mater. Sci. Technol. **105**, 214 (2022)
[45] G.Y. Li, W.M. Jiang, F. Guan, J.W. Zhu, Z. Zhang, Z.T. Fan, J. Mater. Process. Technol. **288**, 116874 (2021)
[46] P.D. Huo, F. Li, Y. Wang, R.Z. Wu, R.H. Gao, A.X. Zhang, Mater. Des. **219**, 110696 (2022)